Effects of smooth boundaries on topological edge modes in optical lattices

Michael Buchhold, Daniel Cocks, and Walter Hofstetter
Institut für Theoretische Physik, Johann Wolfgang Goethe–Universität, 60438 Frankfurt/Main, Germany
(Received 11 April 2012; published 18 June 2012)

Since the experimental realization of synthetic gauge fields for neutral atoms, the simulation of topologically nontrivial phases of matter with ultracold atoms has become a major focus of cold-atom experiments. However, several obvious differences exist between cold-atom and solid-state systems, for instance the small size of the atomic cloud and the smooth confining potential. In this article we show that sharp boundaries are not required to realize quantum Hall or quantum spin Hall physics in optical lattices and, on the contrary, that edge states in a smooth confinement exhibit additional interesting properties, such as spatially resolved splitting and merging of bulk bands and the emergence of robust auxiliary states in bulk gaps to preserve the topological quantum numbers. In addition, we numerically validate that these states are robust against disorder. Finally, we analyze possible detection methods, with a focus on Bragg spectroscopy, to demonstrate that the edge states can be detected and that Bragg spectroscopy can reveal how topological edge states are connected to the different bulk bands.

DOI: 10.1103/PhysRevA.85.063614 PACS number(s): 67.85.−d, 37.10.Jk, 05.30.Fk

I. INTRODUCTION

Ultracold atoms in optical lattices provide a unique experimental setup for studying properties of solid-state systems in a very clean and well-controlled fashion [1,2]. Particularly interesting in this context is the experimental implementation of artificial gauge fields for neutral atoms [1,3–6], simulating, for instance, time-reversal-symmetry-breaking magnetic fields [7–12] or a coupling of the atom's internal spin degree to its angular momentum [13–16]. The realization of these effects will open a path for precise simulations of a large class of topologically nontrivial systems such as quantum Hall (QH) or quantum spin Hall (QSH) phases. Creation of topological states of matter with cold atoms is particularly attractive because of the precise control of physical parameters such as the hopping amplitude and interaction strength, allowing the possibility to observe strongly interacting topological phases in lattice experiments. However, the implementation of artificial gauge fields for neutral atoms is only one experimental challenge in simulating topological phases in optical lattices [17–20]. Experiments must overcome the difficulties provided by the finite size of the lattice and the soft boundary of the system, caused by a trapping potential that is smoothly varying in space. The finite size leads to a finite overlap of spatially separated counterpropagating edge states and therefore to possible backscattering processes, decreasing the robustness of the edge states against external perturbations [21,22]. While this is not a very serious restriction for optical-lattice potentials, which are relatively pure, the effects of the soft boundary of the optical-lattice system may significantly change the properties of the edge states characterizing topological insulators in finite systems. Whereas recent publications identify the soft boundaries as an unwanted restriction or propose ways to avoid them by implementing artificial sharp boundaries in their systems [23], we demonstrate in this article that soft boundaries will lead to interesting additional features, either not present or at least not visible in systems with sharp boundaries. For this purpose, we investigate different trap shapes and geometries, which are realizable in optical lattices, and discuss their specific influence on the cold-atom system.

This article is organized in the following way. First, in Sec. II, we present the theoretical model under consideration, a QH Hamiltonian in the tight-binding approximation for spin-polarized fermions confined in an additional trapping potential. In Sec. III, we present our results for the stripe geometry, discussing in detail the properties of the edge states in systems with a hard-wall boundary, a harmonic trap, and a quartic trapping potential. In Sec. IV, we study the shape of the edge states in a completely trapped system and investigate the suitability of several detection methods as tools to probe the system experimentally, including Bragg spectroscopy. Finally, in Sec. V, we provide some conclusions.

II. THE MODEL

The model we consider is similar to the ones proposed in Refs. [7,11], experimentally realizing time-reversal symmetry breaking topological insulators with ultracold atomic gases. This model describes a two-dimensional (2D) system of spin-polarized fermionic atoms subjected to a square optical lattice, experiencing an artificial Abelian gauge field $\boldsymbol{A}$ that induces an artificial uniform magnetic field perpendicular to the lattice, $\boldsymbol{B} = B\boldsymbol{e}_z$, which is similar to the celebrated Hofstadter Hamiltonian [24] on the lattice. In our system, the gauge field $\boldsymbol{A}$ enters the first-quantized Hamiltonian of the system in the form of the minimal coupling $\boldsymbol{p} \to \boldsymbol{p} - \frac{e}{c}\boldsymbol{A}$, which leads to the Hamiltonian

$$H = \left(\mathbf{p} - \frac{e}{c}\mathbf{A}\right)^2 / 2m + W(\mathbf{x}) + V(\mathbf{x}). \tag{1}$$

The Hamiltonian (1) contains the optical lattice potential W and a spatially dependent scalar potential V which allows for the inhomogeneity of the lattice, caused by the finite width of the laser beams creating the lattice or additional external potentials such as a harmonic trap or an artificial hard-wall boundary. For the moment we leave the detailed shape of V arbitrary, and assume only that the nonlocal matrix elements of V are negligible (i.e., $\langle l|V|m\rangle = \delta_{l,m}\langle l|V|l\rangle$, where $\langle l|$ is the Wannier state at lattice site l), which is reasonable in our

case since the potential is either varying slowly compared to the lattice spacing a or a step function.

The second-quantized form of Hamiltonian (1) in the tight-binding approximation then reads

$$H = -t \sum_{l,m} c_l^\dagger e^{i2\pi\phi_{l,m}} c_m + \sum_l V_l c_l^\dagger c_l . \tag{2}$$

The operator $c_l^\dagger$ here denotes the fermionic creation operator at lattice site l, with its corresponding annihilation operator c_l. The first term is the well-known nearest-neighbor hopping with amplitude t, and is complex due to the Peierls phases $2\pi\phi_{l,m}$ that are a result of the gauge field [24]. The second term corresponds to the inhomogeneity V with the local matrix elements $V_l \equiv \langle l|V|l\rangle$. The phases $\phi_{l,m} = \frac{1}{2\pi}\int_l^m \mathbf{A}\cdot d\mathbf{l}$ are not uniquely defined by the magnetic field and depend on the gauge chosen. In this paper, we choose the common Landau gauge $\mathbf{A} = (0, Bx, 0)$, which leads to $\phi_{l,m} = \alpha x_l(\delta_{y_l,y_m+1} - \delta_{y_l,y_m-1})$, where x_l and y_l are the coordinates of lattice site l with lattice spacing $a = 1$ and $\alpha = \frac{\Phi}{\Phi_0}$ represents the flux per plaquette in units of the magnetic flux quantum $\Phi_0 = h/e$. Setting $e = \hbar = 1$, we obtain $\alpha = \frac{B}{2\pi}$ for the square lattice. Throughout the rest of this article we choose the hopping t as the natural energy unit of our system.

In the following sections we will restrict our analysis to the case where $\alpha = 1/6$ or $2/5$. Our results for these two cases can easily be generalized to other cases where $\alpha = p/q$, with $p,q \in \mathbb{N}$, and where topological edge states are predicted [25].

The experimental realization of a similar model was proposed in Ref. [23], where the authors consider a spinful fermionic system subjected to an artificial gauge field that simulates a magnetic field of the form $\boldsymbol{B} = B\sigma\boldsymbol{e}_z$, where $\sigma = \pm 1$ is the spin quantum number. This model preserves time-reversal invariance and therefore allows for the realization of QSH phases in optical lattices. Because of the time-reversal symmetry, our analysis also applies to this model when spin remains a good quantum number, and we will mention the corresponding QSH phases throughout the text. So far, we have not accounted for a Zeeman splitting due to an external magnetic field, a spin-orbit coupling, or a staggering potential, all realizable in optical lattices [23]. The physics caused by these additional effects are indeed very interesting and leaving them out may seem quite restrictive, but the results we discuss in this article are quite general and require only that the states are topological and do not rely on the detailed nature of the edge states.

III. EDGE STATES IN CYLINDRICAL GEOMETRIES

The defining property of topological insulators in a semi-infinite system is the emergence of gapless edge states which are localized at one edge and robust against perturbations of the system, e.g., potential or magnetic disorder. Furthermore, the presence of these states is the origin of the currents measured in QH [25–27] and QSH samples [28–30] which are well known to be strictly quantized when S_z is a good quantum number. Topological phases are typically distinguished by the transport properties of the edge states, specifically by the quantized charge (or mass for neutral atoms) that is transported at a single edge [31,32]. One method of determining the topological quantum number for a given system is therefore to calculate the energy spectrum on a cylindrical geometry and to evaluate the transport properties of the edge states directly. Alternatively, one may determine the topological quantum numbers from the dispersion relation of filled bands [35] or the corresponding eigenstates [32–34] in the corresponding infinite system.

In this section we will focus on a cylindrical geometry and determine the spectral functions of the system of interest via exact diagonalization of the Hamiltonian for a finite system of size 100×100 [36]. We discuss the properties of the edge states of the system by analyzing the integrated spectral function in quasimomentum space and real space for several kinds of boundaries and show the robustness of the edge states against perturbations by switching on a disordered potential.

A. Identification of topological invariants

Topological phases can be characterized either by analyzing the band structure properties of the infinite system, or in terms of the transport properties of the system in a confined geometry. While the first approach is insensitive to the specific shape of the confining potential, the latter may in principle strongly depend on these details. In this section we discuss the properties of edge states at an infinite wall boundary, realized by open boundary conditions at the edges of the cylinder, henceforth referred to as stripe geometry. For this kind of boundary the topological quantum number of the infinite system is equivalent to the transport coefficient ν of the finite system, a relation known as the bulk-boundary correspondence [34,35]. The coefficient ν counts the difference in number of forward-moving and backward-moving states at the Fermi edge, which represents the net transport for low-energy excitations and hence the quantized edge current I_E [25]. Explicitly, we have [37]

$$\nu_m = \sum_{\alpha_m} \mathrm{sgn}\big[\partial_{k_y}\epsilon_{\alpha_m}(k_y)\big], \tag{3}$$

where α_m labels the states at the Fermi edge with energy $\epsilon_{\alpha_m}(k_y) = \epsilon_F$ and $m = L, R$ for the left and right edge, respectively. Equation (3) can be obtained by applying the well-known Laughlin argument to a cylindrical geometry and subsequently following the procedure described in Ref. [34], where no details of the trapping potential are required. For the gauge $\mathbf{A} = (0, Bx, 0)$, the single-particle Hamiltonian (1) obeys the symmetry $H(\mathbf{x},\mathbf{p}) = H(-\mathbf{x}, -\mathbf{p})$, which leads to $\nu_L = -\nu_R$. Throughout this article we will only consider the Hall transport coefficient for the left edge $\nu \equiv \nu_L$, which is identical to the topological $\mathbb{Z}$ quantum number of the infinite system and determines the Hall conductance $\sigma_{xy} = \nu e^2/h$. The topological $\mathbb{Z}_2$ quantum number ν_2, which indicates QSH phases in the corresponding spin-1/2 system [23], can then be obtained, if S_z is a good quantum number, by Refs. [38,39]

$$\nu_2 = |\nu| \bmod 2. \tag{4}$$

If $\nu_2 = 1$ the system will exhibit a QSH phase.

In this paper we make an explicit distinction between an "edge state" and an "edge mode." An edge state always refers to an eigenstate of the Hamiltonian that is localized to one edge, whereas an edge mode refers to a series of edge states that are smoothly connected in momentum space. Although

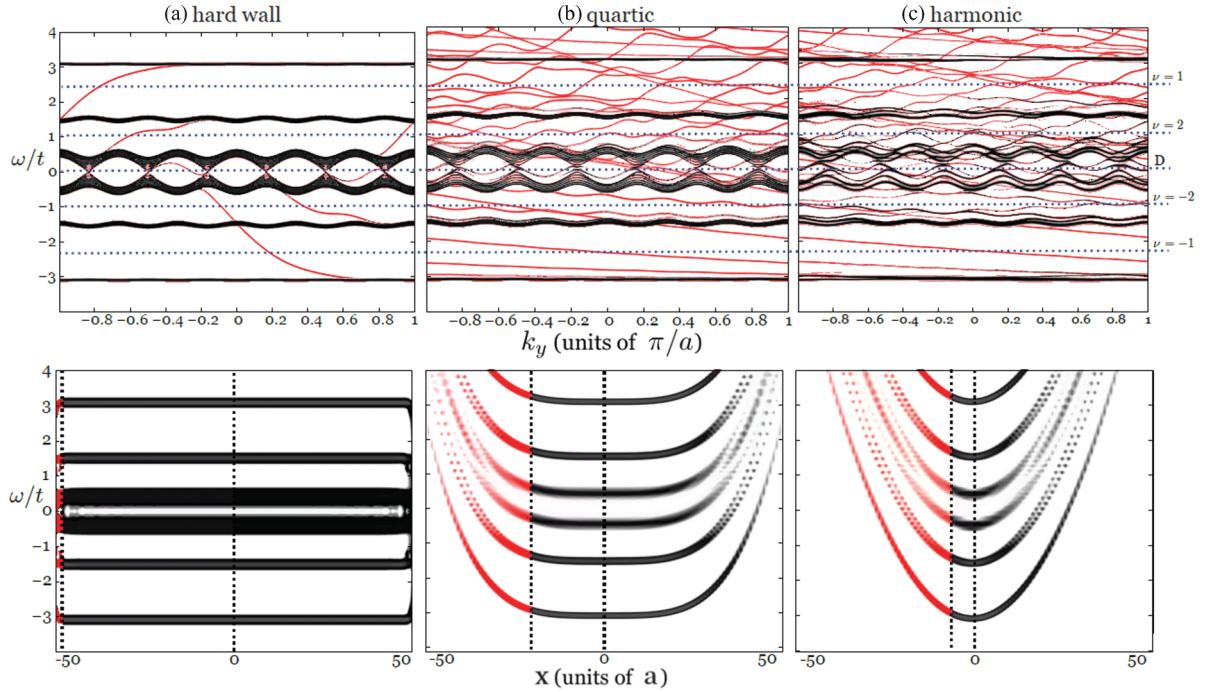

FIG. 1. (Color online) Integrated spectral function for a system described by Eq. (2) with flux $\alpha = 1/6$ and stripe geometry with 100×100 lattice sites [36]. Three experimentally relevant confinements of the form $V(x) = V_0(x/L)^\delta$ are shown: (a) hard-wall confinement, $\delta \to \infty$, (b) quartic confinement, $\delta = 4$, and (c) harmonic confinement, $\delta = 2$. The spectra in the upper row, $\rho_L(k_y,\omega)$, show the k_y dependence along the periodic direction, integrated over the left half of the confinement direction (see text), and the real-space spectra of the lower row, $\tilde{\rho}(x,\omega)$, show the x dependence along the confinement direction. To the right of the figure are the transport coefficients, calculated using (3) with the Fermi edge set to the corresponding dotted line. For hard-wall and quartic confinement there is an appreciable number of bulk bands and the edge states are clearly distinguishable, whereas within harmonic confinement we consider almost all of the states to be edge states. In each case we indicate left-edge states in red, while the remaining bulk states are shown in black, corresponding to the left half of the cylinder in real space (see lower plots). Two possible approaches exist for designation of edge and bulk states in softly confined systems. As seen in the upper row, energy regions with well-defined topological quantum numbers can be identified in the spectrum. The corresponding states can be designated as part of the edge, and the remaining ones as the bulk. Alternatively, we can define the edge as the point at which no states have energies within the range of energies covered by states at the center of the trap. We use the latter designation, although there is little difference between the two methods.

this distinction is not necessary for hard-wall systems, it is required for soft-boundary systems.

B. Cylindrical geometry with open boundary conditions

We first consider a system described by Eq. (2) with a step potential V that is zero for $|x| \leqslant L_x/2$ and infinite elsewhere, with L_x sufficiently large, providing a hard-wall boundary at the edges of the cylinder. Since the quasimomentum in the y direction is a well-defined quantum number and we are interested in transport coefficients for this direction, it is convenient to represent the spectrum of the system in terms of the integrated spectral density $\rho_L(k_y,\omega) \equiv \int_{-L/2}^{0} dx\, \rho(x,x,k_y,\omega)$, where the spectral function is defined as

$$\rho(x,x',k_y,\omega) = -2\mathrm{Im}\langle x,k_y|\frac{1}{\omega - H + i0^+}|x',k_y\rangle. \qquad (5)$$

We integrate only over the left half of the system in real space, so as to separate the left from the right edge states [40]. In Fig. 1(a), upper panel, the integrated spectral density $\rho_L(k_y,\omega)$ is shown for $\alpha = 1/6$. One can identify the bulk states, which are grouped into six thick bands, and the edge states, which close the gaps between the bands. To determine the transport coefficients and possible topological phases, we place the Fermi edge in a bulk gap and apply (3) to the dispersion of the edge states.

There are several phases visible in this system. If the Fermi edge lies within a bulk band, the system is in a trivial metallic phase. If the Fermi edge lies between the third and fourth bands, there is a set of Dirac points with a linear dispersion and the phase is a semimetal. In the bulk gaps, which lie between the other bands, the edge modes place the system in a quantum Hall state with $\nu = -1$ and -2 for the first and second bulk gaps, respectively, and inverted for the third, fourth bulk gap. In shorthand, we can specify the phases between the bands by $\mathrm{gap}_{1/6} = \{-1,-2,D,2,1\}$, where D represents the Dirac points. In the analogous spin-1/2 system, $\nu = \pm 1$ indicates a QSH phase whereas $\nu = \pm 2$ corresponds to a normal insulator, due to lack of topological protection.

In addition we also investigate the case where $\alpha = 2/5$ (see Fig. 2) for which we find $\mathrm{gap}_{2/5} = \{2,-1,1,-2\}$. Note that there are no Dirac points for $\alpha = 2/5$. The differences between $\mathrm{gap}_{1/6}$ and $\mathrm{gap}_{2/5}$ appear as different real-space behaviors within soft confining potentials that are not visible within a hard-wall confinement, as we demonstrate in the next section.

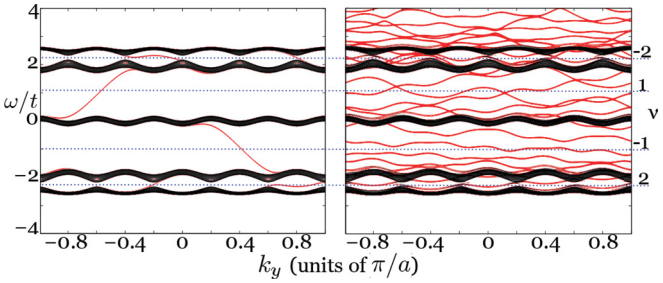

FIG. 2. (Color online) Integrated spectral function $\rho_L(k_y,\omega)$ for a system described by Eq. (2) with flux $\alpha = 2/5$ and hard-wall (left) and quartic (right) confinement. Edge states are shown in red, while bulk states are shown in black.

C. Cylinder with soft boundaries

With soft boundaries, it becomes relevant to look at the spectra of the system in real space along the x axis, $\tilde{\rho}(x,\omega) = \int dk_y\, \rho(x,x,k_y,\omega)$, as well as the partially integrated spectra in quasimomentum space along the k_y axis, $\rho_L(k_y,\omega)$. The quasimomentum spectra allows us to extract transport coefficients and discuss the dispersion of the edge modes. On the other hand, the real-space spectrum exhibits some unusual features for different trapping conditions. We consider a lattice of size 100×100 [36] and trapping geometries of the form $V(x) = V_0(x/L)^\delta$, where $V_0 = 10t$ and $L = 50a$ is chosen such that $V(x = 50a) = V(x = -50a) = 10t$ which is larger than the energy spanned by the infinite system $\sim 8t$. Three particular values of δ are relevant to experiment: $\delta \to \infty$, which reproduces hard-wall boundary conditions, $\delta = 4$ for quartic confinement, and $\delta = 2$ for harmonic confinement. In most optical-lattice experiments, the confining potential is a result of the Gaussian envelope of the finite beamwidth of the lasers and in the center of the trap we may approximate this confinement by its leading-order harmonic term. However, it is has been suggested [41] that one can remove the harmonic term by superimposing an antitrapping Gaussian beam of different detuning on the trapping beam, which then promotes the quartic term to the leading-order approximation of the trapping potential, i.e., $V(x) \propto x^4$. This scheme was realized in optical-lattice experiments to improve quantum phase diffusion experiments [42,43]. We investigate these trapping geometries below in further detail.

1. General features and preservation of topological invariants

In Fig. 1, we show a comparison between $\rho_L(k_y,\omega)$ and $\tilde{\rho}(x,\omega)$ for $\alpha = 1/6$ and hard-wall, quartic, and harmonic confinements that are relevant to experiment. One can see that the potential does not gap the system, and edge modes continue to connect the bands. The transport coefficients of the soft-boundary systems, indicated to the right of Fig. 1, are insensitive to the trapping potential. In other words, there exist energy ranges in which we can identify a transport coefficient, which is identical for all confinements we consider.

Comparing the k_y-dependent soft-boundary spectra of the upper row in Fig. 1, we make two observations: (1) we can readily identify highly degenerate regions of bulk bands in the hard-wall and quartic confinements, and (2) we find that the dispersion of edge modes that are present within quartic confinement does not change noticeably whenthe confinement is changed to the harmonic trap. In contrast, the rest of the spectrum is significantly modified, such that the ratio of bulk to edge states is very small. To define such a bulk region in the soft-boundary system, we assume that the edge begins at a distance from the trap center where none of the states at this point overlaps in energy with any of the states in the very center of the trap (i.e., at $x = 0$).

Analogously, we can clearly identify a bulk region from the x-dependent spectra in the bottom row of Fig. 1 for the quartic trap, but not in the case of the harmonic trap. From this we conclude that the quartic trap is likely the best trapping potential for observing effects of both the bulk system and topological edge states in an experimental setup, if it is not feasible to artificially implement hard-wall boundaries as proposed, for example, in Ref. [23]. Furthermore, we observe no overlap between states of different edges, which has been proposed to destroy edge states via couplings between the edges [21]. This again shows that the edge states are topologically protected and robust against external changes in the potential.

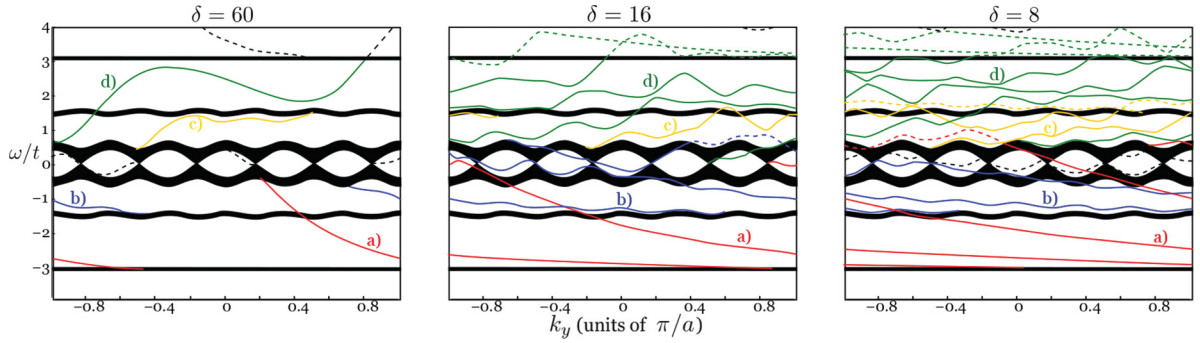

FIG. 3. (Color online) False color diagram of the integrated spectral density $\rho_L(k_y,\omega)$ for a system described by Eq. (2) with flux $\alpha = 1/6$, stripe geometry, and a confining potential $V(x) = V_0(x/L)^\delta$. Bulk bands are indicated in black and edge modes as colored curves, also marked as (a), (b), (c), (d). There exist several true crossings and avoided crossings in the spectra which combine to preserve the topological invariants for any confinement exponent δ. Auxiliary states of the corresponding edge modes are shown with dashed curves. The auxiliary states do not influence the topological phases of the system, since they always come in pairs with opposing velocities.

In Fig. 2, we also show a comparison of $\rho_L(k_y,\omega)$ for the case where $\alpha = 2/5$ between a hard-wall (left column) and a quartic confined system (right column). We again calculate the transport coefficients of both systems and list these next to the plots to show that these also coincide for all trapping potentials.

To better understand the details of the rather complicated spectra of the quartic trap, we choose to follow the edge modes of the hard-wall confinement by smoothly varying the trapping exponent δ. We show plots for $\delta = 60,16,8$ and $\alpha = 1/6$ in Fig. 3, where we have artificially colored the spectra to indicate each edge mode. $\delta = 60$ represents a very steep trap, and is almost identical to the hard-wall case: with the color designation, one sees that the blue and yellow edge states are present only in the second and third bulk gaps, respectively, whereas the red (marked as (a)) and green edge states (d) span two bulk gaps. As the confinement is made softer, we see that an edge mode may cross the Brillouin zone more than once, and that the energy range of the edge states changes, e.g., with $\delta = 8$ the red state (a) now extends into the third bulk gap. However, whenever this occurs, the state forms an avoided crossing at some higher energy with a different edge state and is forced downward in energy, a process which preserves the value of the topological invariants. We represent this in the false color diagram by a dotted line for parts of the edge states that are nontopological, i.e., not connecting different bulk bands. For $\delta = 16,8$, we can consistently see this occurring in the most energetic edge mode (colored green, (d)), which extends above the highest bulk band, and forms an avoided crossing with the nontopological edge state created by the effect of the trapping on the highest bulk band.

Note that, due to the trapping potential, several edge states that belong to the same edge mode may exist for one value of energy.

2. *Merging and splitting of edge states*

When the number of edge modes changes, as the Fermi edge crosses a bulk band in the hard-wall boundary system, either an edge mode must be created, or an edge mode must merge either into the bulk band itself or with another edge mode. In the soft-boundary system we can see some very nontrivial behavior that shows the complexity of these processes.

We first focus on the real-space spectra of the $\alpha = 2/5$ flux system under quartic confinement; see Fig. 4. In the lowest gap, we see that two different edge modes, which evolve between the first and second bulk bands, merge into a single edge mode, which evolves between the second and third bulk bands. In the hard-wall system, this mode is localized to a single site in the x direction and can be observed only in quasimomentum space. In the quartic trap, the edge states leaving the first bulk band follow the shape of the quartic potential and one may expect the same for the states leaving the second bulk band. As one sees in Fig. 4, this is not the case. The states leaving the second bulk band immediately start to merge with the edge states from the first bulk band, and the result is only a single mode at each edge, evolving between the second and third bulk band. Although it is not possible to determine topological invariants from real-space spectra, we can link this merging behavior to the k_y-space spectra of Fig. 2 and see that it leads

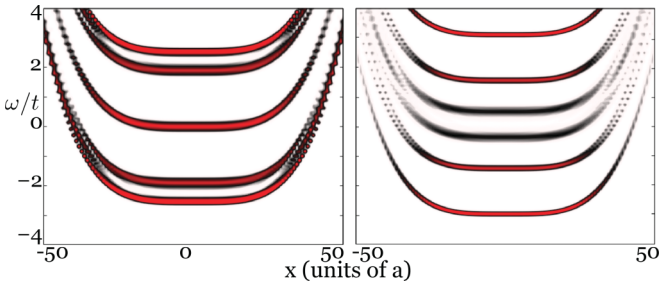

FIG. 4. (Color online) Integrated spectral density $\tilde{\rho}(x,\omega)$ for a system described by Eq. (2) on a 100×100 lattice with quartic confinement V. In the left figure, the flux is chosen to be $\alpha = 2/5$, while in the right figure $\alpha = 1/6$. In the left figure, the edge states leaving the second bulk band immediately merge with the edge states of the first bulk band to form a state spatially localized between the bulk bands with the correct transport coefficient. In the right figure, the states leaving the second bulk band split up, i.e., they localize to more than one point in space. The inner part of these states merges with the edge states of the third band at higher energies. Similar behavior is observed for the third, fourth, and fifth bands. As pointed out in the text, this nontrivial behavior is an indication of the topological origin of the edge states.

to the correct topological quantum number $\nu = -1$. The same effect is again observable between the fourth and fifth bulk bands. Interestingly, the merging of these modes does not take place via a simple overlap of the states, but a gap in real space with negligible spectral weight exists between the states originating from the bands and the newly formed edge mode.

In the $\alpha = 1/6$ flux system, we also see the opposite effect: the splitting of a single bulk band, to connect edge modes of different bands which are energetically well separated. In Fig. 1, the integrated spectral density $\tilde{\rho}(x,\omega)$ shows that the modes leaving the second and fifth bulk bands each split into two curves, where a single eigenstate has large amplitudes on two spatially separated lattice sites. We interpret this splitting as a process that facilitates the connection between different bands which we observe in Fig. 3. For example, the outer part of the mode leaving the second bulk band can be seen to merge at higher energies with the mode that is a product of the third and fourth bands. This connection between the bands is analogous to the avoided crossings that we observe in the k_y-dependent spectra in Fig. 3. This very nontrivial behavior of modes within the outer region of the system, combined with transport coefficients which are identical to the topological quantum numbers, given by the transport coefficients of the infinite system, indicates that the soft edge states are of topological origin. To further verify this, we address in Sec. III D the robustness of these states against perturbations in terms of a disordered background potential.

3. *Relation of edge states and bulk bands*

When we look more closely at the dispersion of the edge modes, we can see an interesting connection to the bulk bands of the system. We focus on the quasimomentum spectra for the case $\alpha = 1/6$ shown in Fig. 3 for increasing confinement exponent δ.

The dispersion of an edge mode leaving a given bulk band can be described on two different quasimomentum scales. For a small range of k_y, the dispersion mimics that of its associated bulk band, and this behavior becomes more prominent for smaller δ. This can be seen for the lowest edge modes, colored red (a) and blue (b), e.g., the red (a) mode has a locally flat dispersion, mirroring the flatness of the lowest band. However, when avoided crossings have occurred, such as for the yellow (c) and green (d) edge modes, the dispersion of an edge mode cannot simply be described by one band alone and corresponds to a mixture of bands.

On the other hand, considering the Brillouin zone as a whole, the edge modes become more flat in momentum space the smoother the confining potential is in real space. This flattening is a direct result of the number of accessible sites at the edge. The number of lattice sites, n_{edge}, that are available for an edge state between, e.g., the first and the second bulk bands, is the number of sites i that fulfill $\epsilon_1 - \epsilon_0 \lessapprox V(x_i) \lessapprox \epsilon_2 - \epsilon_0$, where ϵ_1 (ϵ_2) are the maximum (minimum) energies of the first and second bulk band, respectively, and ϵ_0 is the minimum energy of the first bulk band [22]. In the hard-wall system, $n_{\text{edge}} = 1$, but becomes larger as the confining potential becomes smoother in real space. An interesting result for the $\alpha = 1/6$ flux per plaquette is that the flatter the potential becomes, the flatter the lowest gap edge modes become, with a corresponding increase of the effective mass of the system's excitations:

$$m^* \equiv \left(\frac{\partial^2}{\partial k_y^2} \epsilon(k_y) \right)^{-1} \to \infty. \tag{6}$$

This is generally true for soft confinements, as pointed out in Ref. [22], but the edge-state structure in the case $\alpha = 1/6$ allows this feature even for relatively steep potentials.

D. Robustness of soft edge states in stripe geometries

One of the most important properties of topological edge states is their robustness against even large perturbations, which leads to clearly detectable quantized Hall conductance in impure experimental setups. In optical-lattice experiments, which are, by construction, very clean realizations of condensed-matter Hamiltonians, perturbations such as disorder are usually not an issue. However, since disordered potentials can be implemented in a controlled manner [44–46], it is of interest to thoroughly investigate how robust the edge states are against these kinds of perturbation. Here, we address this question for soft boundaries. The general argument, which illustrates the robustness of edge states in condensed-matter systems, is the lack of possible backscattering processes [32]. Counterpropagating edge states are localized on opposite edges of the system and are very well separated spatially. Therefore, in huge condensed-matter systems, these states have vanishing spatial overlap and backscattering from impurities is completely suppressed. In contrast, in finite systems different edge states from opposite edges will have a finite overlap in real space, which theoretically allows for backscattering processes, and therefore disorder may lead to the opening of a gap in the spectrum. However, as we will see from our numerical results, even in very small systems

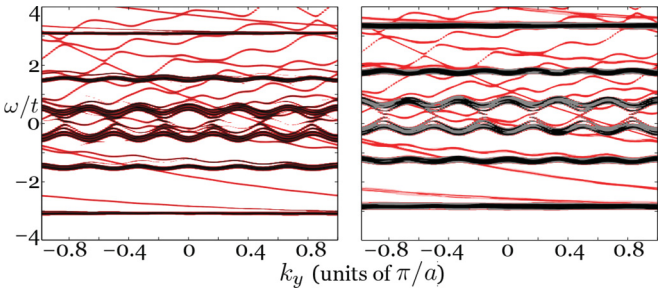

FIG. 5. (Color online) Integrated partial spectral density $\rho_L(k_x,\omega)$ of a system described by Eq. (2) on a 120×60 lattice with $\alpha = 1/6$ [36]. Right: with an additional binary disordered potential, given by Eq. (7) and $\Delta_{\max} = 0.5t$. Left: with the disordered potential being set to zero. The robust edge states are still clearly pronounced and gapless, while the former bulk bands are smeared out and show a mobility gap (not shown here but obtainable from the Anderson-localized bulk eigenstates).

(≈60 lattice sites in the y direction) this effect is not observable.

To verify the robustness of the soft edge states numerically, we perturb the system described by Eq. (2) by adding a disordered background potential

$$V_{\text{disorder}} = \sum_l \Delta_l c_l^\dagger c_l, \tag{7}$$

where Δ_l is distributed randomly, either by a binary distribution, $\Delta_l \in \{0, \Delta_{\max}\}, \forall\, l$, or by a uniform distribution, $\Delta_l \in [0, \Delta_{\max}], \forall\, l$ [47]. For all realizations, we found that the edge states stay robust and still connect the different bulk band regions without opening a gap up to disorder strengths of about $\Delta_{\max} \approx 0.5t$ for binary disorder and even larger strengths for uniform disorder.

For example, in Fig. 5 the integrated partial spectral density $\rho_L(k_y,\omega)$ is shown for a 120×60 lattice system with uniformly distributed Δ_l and $\Delta_{\max} = 0.5t$. There is clearly no gap in the spectrum and although quasimomentum is no longer a good quantum number, the edge states in momentum space are very sharply centered around a particular value of k_y and remain delocalized in the y direction as they were for the system without disorder [48]. In contrast, some of the bulk states now consist of many quasimomentum components (not shown in our figure) and therefore become localized to a region much smaller than the system size, which can be termed Anderson localization.

We have also addressed larger systems with larger boundary regions. These systems contain more and more edge states in a given bulk gap, which may possibly lead to different backscattering processes between edge states located at the same edge and therefore open gaps in the spectrum after disorder is introduced. To exclude these possibilities, we studied system sizes of up to 60×240 lattice sites without finding any indication of gaps in the spectrum or localization of the edge states up to disorder strengths of $\Delta_{\max} = 0.5t$.

IV. DETECTION METHODS

So far we have focused on a semi-infinite system with stripe geometry. However, realistic systems in optical-lattice experiments are confined to a finite region in all dimensions by

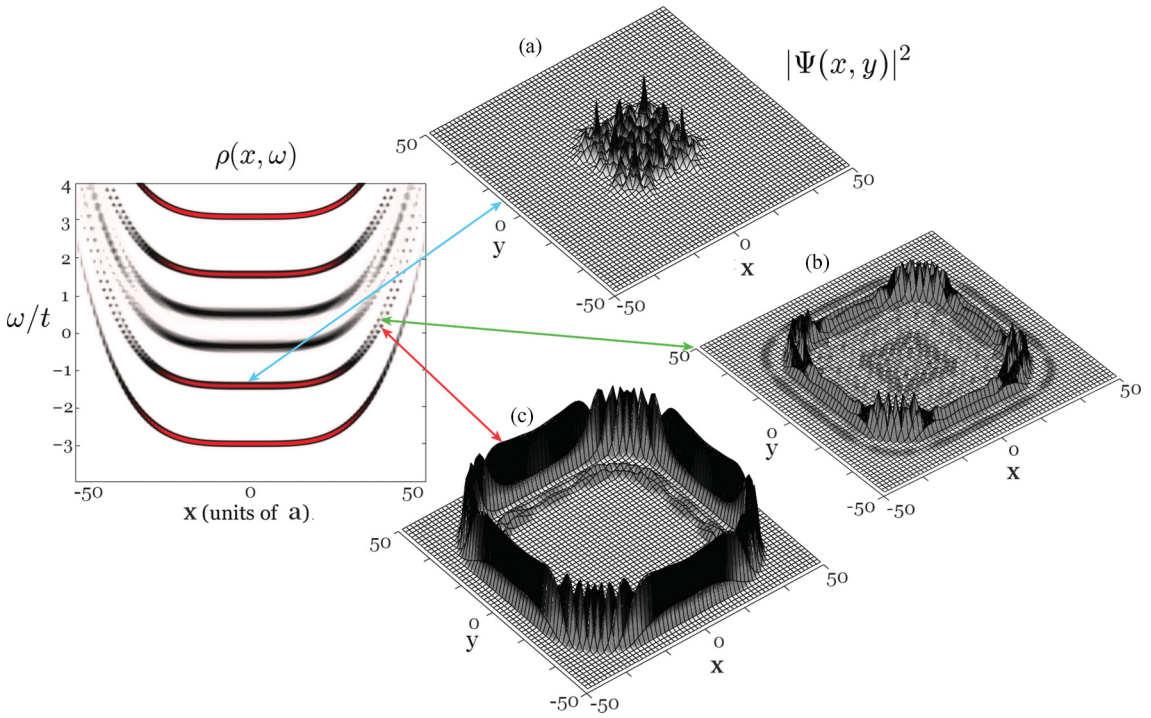

FIG. 6. (Color online) Wave function $|\Psi(x,y)|^2$ as a function of the lattice spacing a of different eigenstates of the system within complete quartic confinement. The real-space spectral density shown to the left is a cross section of the complete system: $\rho(x, y = 0, \omega)$. Three particular eigenstates have been shown, and their energies indicated by arrows to the spectral density. The wave functions belong to (a) a bulk region and (b) and (c) to a pair of edge states splitting up after leaving the second bulk band.

the finite beamwidth of the lasers. In this section, we determine the spatial wave functions of a 2D system trapped in both the x and y directions and discuss possible detection methods of the resulting edge states.

A. Eigenstates of the completely trapped system

We determine the eigenstates of a system with a confining potential V that varies in the x and y directions

$$V(x,y) = V_0\left[\left(\frac{x}{L}\right)^{\delta} + \left(\frac{y}{L}\right)^{\delta}\right]. \tag{8}$$

The parameter δ determines the shape of the trap and the possible eigenstates. For $\delta \to \infty$ the system is again confined by hard walls in both directions, while for $\delta = 4$ and $\delta = 2$ the system is in a quartic and a harmonic confinement, respectively. For harmonic confinement, we expect the eigenstates that are extended over various lattice sites to be circularly symmetric, whereas in the quartic case the potential is no longer circularly symmetric and the states take on a shape that is sometimes referred to as a squircle [49]. For this analysis we again will restrict ourselves to a system with 100×100 lattice sites and a trapping potential with a minimum value of $V_0 = 10t$ along each edge of the lattice. We again focus on $\alpha = 1/6$.

In Fig. 6, we clearly see the different real-space distribution of edge states compared to bulk states. The bulk states are delocalized over a region of about 30×30 lattice sites, while the edge states for a given energy follow the isolines of the quartic potential, and are strongly confined to these regions. Comparing Figs. 6(b) and 6(c) for the completely trapped system one can see the splitting of the edge states leaving the second bulk band as the two states have a weak overlap with one another. The shape of the edge states in the quartic confinement looks similar to that which one would expect in the hard-wall system (like those explicitly shown in Ref. [50]) and differs only at the very corners of the system. We therefore expect similar single-particle excitations for the quartic confinement as for the hard-wall confinement when probing the edge states in experiment.

The situation slightly changes for the harmonically confined system. There, the confining potential is circularly symmetric and one may expect that the eigenstates reflect this symmetry. The wave functions of the harmonically confined system are shown in Fig. 7. As already seen from the spectral density plotted in Fig. 1, the former bulk region is tightly confined to very few lattice sites in the center of the trap, which makes it difficult to define a bulk region in the harmonic trap. On the other hand, the edge states chosen reflect the radial symmetry of the trapping potential and again are localized along the isolines of the trapping potential. This already indicates that for the harmonic confinement we expect very different excitation dynamics than for the quartic and hard-wall confinement, where significant parts of the eigenstates are quasi-one-dimensional.

For harmonic confinement, one can solve the continuum model analytically in the absence of the lattice [51,52] and the resulting wave functions are quite similar to those from the lattice calculation. The major difference in the continuum case is that no edge states from different bulk bands merge,

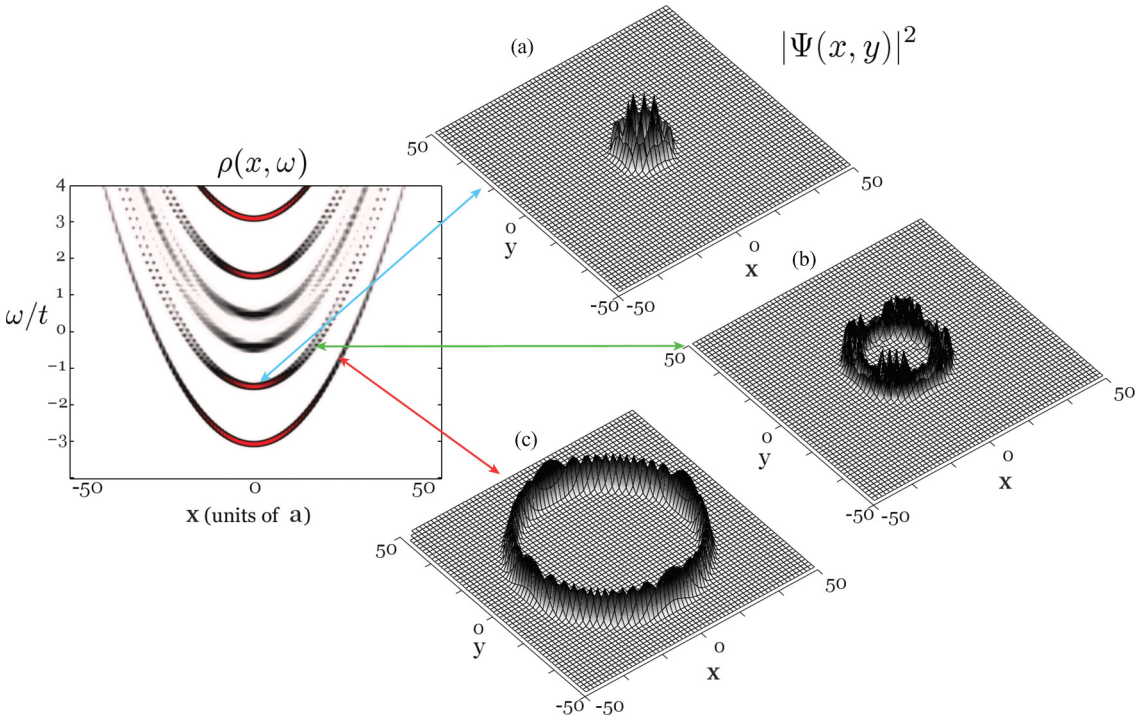

FIG. 7. (Color online) As in Fig. 6 but with complete harmonic confinement. The three states are shown from (a) a bulk region and (b) and (c) edge states of states belonging to different bulk bands. Spatial coordinates in units of the lattice spacing a.

since the Hall conductivity always increases by 1 when passing a bulk band and the different bulk bands are not connected. Additionally, angular momentum is a good quantum number only in the continuum case.

B. Bragg spectroscopy

An important question concerning topological nontrivial phases in ultracold atoms is whether the edge states are detectable with existing experimental tools. Due to the lack of stationary transport in optical-lattice experiments, it is not feasible to directly measure the Hall conductance, and one has to consider alternative approaches [22,53]. Several possibilities for detecting edge states or topological quantum numbers in optical-lattice experiments have been proposed. Some require careful experimental implementation such as Bragg [54,55] or Raman spectroscopy [56], and others take advantage of easily accessible observables like time-of-flight (TOF) patterns or density profiles.

Density profile measurements were proposed by Umucalilar *et al*. [57] to directly separate the bulk and edge densities between different bands. However, as already pointed out in Ref. [22], these profiles do not show the required structure, as can be seen in Fig. 1 (lower panels): the bulk bands all occupy approximately the same real-space extent. Hence, this method is not applicable to topological systems in general.

Alternatively, TOF measurements have been proposed by Zhao *et al*. [58] to exhibit minima and maxima that depend on the topological number of the system. While this is true for the specific cases they were investigating and also for our system in the case of $\alpha = 1/6$, we found that it is not valid in the case of $\alpha = 2/5$ and therefore cannot be reliably used as a detection method in experiment. In contrast, Alba *et al*. [59] propose using TOF measurements as a method to identify skyrmions, by focusing on topological properties of pseudospin vectors within the Hamiltonian on the Bloch sphere. However, this method focuses on bulk properties rather than the edge modes that we consider here.

We choose to focus instead on Bragg spectroscopy, which probes the dynamical structure factor $S(q,\omega)$ of the underlying system. Bragg scattering of topological insulators in optical lattices has been previously considered for the case of the quantum anomalous Hall effect [54]. However, no inhomogeneity of the lattice was considered. Recently, Goldman *et al*. [55] have investigated Bragg spectroscopy theoretically, considering shaped lasers to probe angular momentum states within circularly symmetric traps. While this is a novel implementation to enhance the detection of edge states, we demonstrate that one is able to observe edge states using a simple linear Bragg coupling which, due to technical limitations, may be the only option available to a particular experiment. Furthermore, one can observe differences in Bragg spectroscopy between the various bands that we show is not due to chirality considerations. We do not propose an explicit experimental setup and simply assume that one can measure the dynamical structure factor directly. One such proposal to measure this precisely in an optical lattice is the so-called shelving method [55].

When performing Bragg spectroscopy, the system is illuminated by two laser beams, described by wave vectors $\boldsymbol{p}_1, \boldsymbol{p}_2$ and frequencies $\omega_1 = p_1 c$, $\omega_2 = p_2 c$, respectively, and the differences in these quantities, $\boldsymbol{q} = \boldsymbol{p}_1 - \boldsymbol{p}_2$ and $\omega = \omega_1 - \omega_2$, allow for transitions between different eigenstates of the original system. The Hamiltonian describing the interaction of

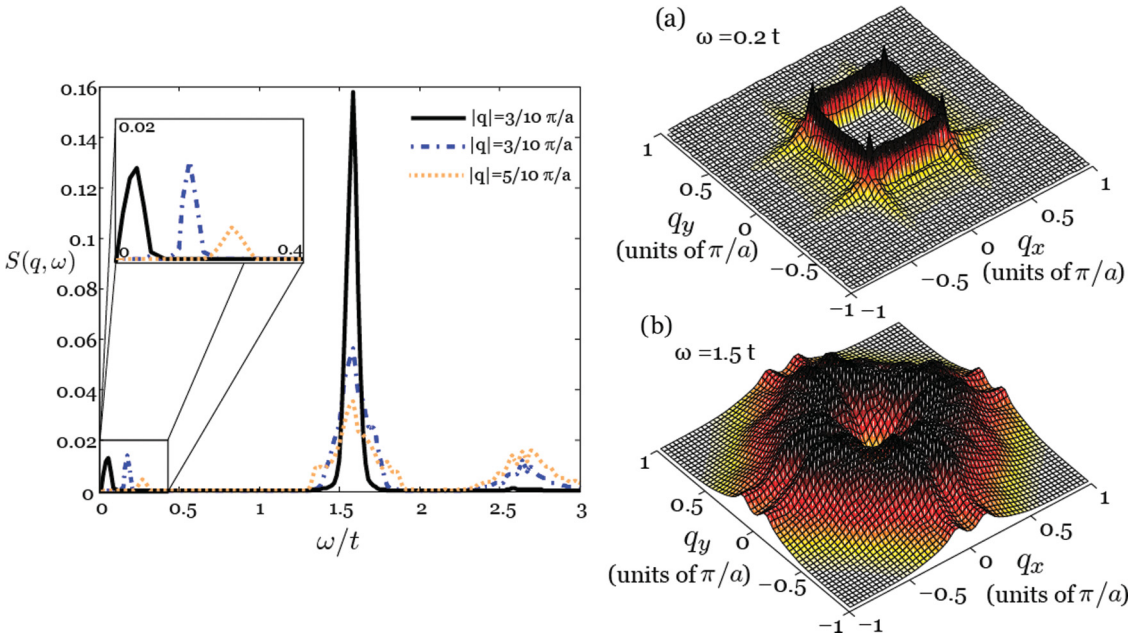

FIG. 8. (Color online) Dynamical structure factor for a system with quartic confinement and Fermi energy in the first bulk gap ($\epsilon_F = -2t$). Left: $S(q,\omega)$ for fixed momentum q as a function of ω. The first peak belongs to edge → edge scattering and its position is sensitive to q and can be written, for small ω, as $\omega_q = v_{F,\mathrm{edge}} q$. The second and third peaks belong to edge → bulk scattering from edge states into the third and fourth bulk bands, located around $\epsilon = 0$, and to bulk → bulk scattering from the first to the second bulk band, where the frequency is independent of q. No signal appears of scattering from edge states to the second bulk band, located at $\omega = 0.5t$, indicating a disconnection between these states, i.e., these states have vanishing matrix elements of the Bragg operator. Right: $S(q,\omega)$ for fixed frequency as a function of momentum transfer q for (a) edge → edge scattering at $\omega = 0.2t$, and (b) bulk → bulk scattering processes at $\omega = 1.5t$.

the system with the laser beams is then given by

$$H_{\mathrm{Bragg}} = \frac{\Gamma}{2}\int d^2p[e^{-i\omega t}\Psi^\dagger(\boldsymbol{q}+\boldsymbol{p})\Psi(\boldsymbol{p}) + \mathrm{H.c.}], \qquad (9)$$

where $\Psi^\dagger(\boldsymbol{p})$ is a field operator creating a particle with real momentum $\boldsymbol{p}$ and Γ is the coupling strength of the lasers [60–62].

The dynamical structure factor in linear response theory for an infinite homogeneous system is directly connected to the density-density correlation function $\chi_{q,q}(\omega)$,

$$S(q,\omega) = -\frac{1}{\pi}\mathrm{Im}\chi_{q,q}(\omega), \qquad (10)$$

via the fluctuation-dissipation theorem [63]. For our case, we have to evaluate $S(q,\omega)$ for the inhomogeneous system, where the quasimomentum is no longer a good quantum number. Within the linear response approximation and accounting for the finite size of the system and finite time of the measurement process, we find

$$S(q,\omega) = |\Gamma|^2\Delta\sum_{\mu,\lambda}\frac{n_\lambda(1-n_\mu)|A_{\lambda,\mu}(q)|^2}{(\omega-\omega_\mu+\omega_\lambda)^2+\Delta^2}. \qquad (11)$$

Here, λ,μ label the single-particle eigenstates of the system, and n_ν and ω_ν are the occupation number and energy, respectively, of the state ν. We introduce a Lorentzian broadening factor Δ, to allow evaluation in a system of finite size. The scattering amplitude $A_{\lambda,\mu}(q)$ is the probability of a particle in state μ to scatter into the state λ by gaining momentum q and is given by the integral

$$A_{\lambda,\mu}(q) = \int d^3r\, e^{-iqr}\psi^*_\mu(r)\psi_\lambda(r). \qquad (12)$$

After determining the single-particle eigenstates of the system, we can directly calculate the dynamical structure factor. Because we are focusing on the detection of edge states, we investigate a system with a Fermi energy located in a bulk gap at $\epsilon_F = -2t$ (see Fig. 1), where an edge state is located. There are now four general scattering processes possible, edge → edge, edge → bulk, bulk → edge, and bulk → bulk. Edge → edge scattering is clearly distinguishable by analyzing the dynamical structure factor. Given a frequency ω, the set of possible momentum transfers allowed to another edge state is very limited because the edge states are well localized in momentum space. For the case of edge → bulk scattering, many different momenta are accessible and therefore we see a signal regardless of the value of q. This means that, for a fixed momentum transfer $\boldsymbol{q}$, $S(\boldsymbol{q},\omega)$ as a function of ω consists of a δ peak approximately around $\omega = q v_F$ [64] and a smeared-out region where the bulk bands are located. This can be seen in Fig. 8 (left), where the first peak indicates edge → edge scattering and the second and third peaks correspond to edge → bulk and bulk → bulk scattering.

On the other hand, for a fixed frequency ω, the response in momentum space describing edge → edge scattering looks quite different from that obtained from edge → bulk scattering, as one can see from Figs. 8(a) and 8(b), respectively. For the quartic confinement, the edge states form squircles in real space (Fig. 6), which means that low-energy excitations

are most favourable in the x or y direction, resulting in the squarelike structure of $S(q,\omega)$ in Fig. 8, which is approximately described by $\{q_{\text{allowed}}\} = \{(q_x,q_y)|\max\{|q_x|,|q_y|\} \approx q_0 = v_F/\omega\}$. In contrast, the dynamical structure factor of bulk → bulk scattering from the first to the second band is smeared out and depends on the Fermi surface of the occupied level at ϵ_F and the Fermi surface of the unoccupied band $\tilde{\epsilon}_F = \epsilon_F + \omega$. The allowed momenta are approximately described by $\{q_{\text{allowed}}\} = \{(q_x,q_y)||q_x| + |q_y| \approx \tilde{\epsilon}_F/\tilde{v}_F\}$ and form a rough square which is rotated by $\varphi = \pi/4$ compared to results for edge → edge scattering. Note that as a result of the structure of $A_{\mu,\lambda}(q)$, where a minimal spatial overlap of the two spatial wave functions is needed to obtain a finite scattering amplitude, high-frequency edge → edge scattering is exponentially suppressed because the presence of the trap causes energetically separated edge states to be localized to different distances from the center of the trap. This does not occur in the equivalent hard-wall system.

For the harmonically confined system, $S(q,\omega)$ as a function of ω for fixed q is qualitatively the same as in the quartic system. In contrast, $S(q,\omega)$ as a function of q for fixed ω for edge → edge scattering looks quite different than for quartic confinement. As seen in Fig. 7, the edge states have a circular symmetry and therefore no momentum transfer direction is preferred, which leads to the set of allowed states forming a circle $\{q_{\text{allowed}}\} = \{(q_x,q_y)|\sqrt{q_x^2+q_y^2} \approx \omega/v_F\}$, shown in Fig. 9.

An important result of our calculations is that there is an obvious absence of spectral weight at frequencies where we expect signals of edge → bulk scattering. To highlight this, we calculate an artificial Bragg response where we allow only initial states in the energy range $-2.5t < \epsilon < -2t$ for transitions to states of higher energy. This means any signal due to possible bulk → edge or bulk → bulk transitions is suppressed. The spectra shown in Fig. 10 demonstrate an edge → edge signal for the first bulk gap and an edge → bulk signal to the third and fourth bulk bands, but conspicuously absent is the signal for the edge → second bulk band transitions, which would be expected for Bragg frequencies $0.5 < \omega < 1.5$. This implies that the first edge and second edge or bulk are disconnected,

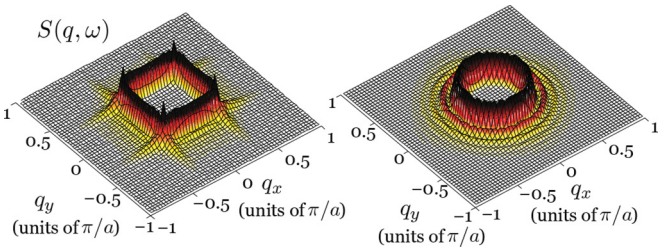

FIG. 9. (Color online) $S(q,\omega)$ for a fixed frequency $\omega = 0.2t$ as a function of momentum transfer q, for a Fermi energy $\epsilon_F = -2t$. Left: $S(q,\omega)$ for the quartic confined system. The system shows a strong response when one component of $q = (q_x,q_y)$ has an absolute value $|q_{x,y}| = q_0 = \omega/v_F$ because excitations along the x and y axes are most favorable (see Fig. 6). Right: $S(q,\omega)$ for the harmonically confined system. Here, the response is close to circularly symmetric in q space, reflecting the shape of the eigenstates. No particular direction is favorable anymore, as long as the absolute value of $|q| = q_0$ is fixed.

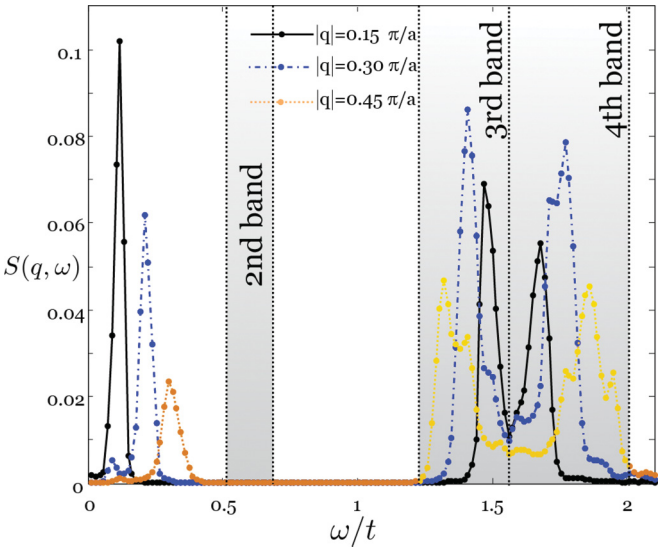

FIG. 10. (Color online) Dynamical structure factor $S(q,\omega)$ for fixed momentum q as a function of frequency, for a Fermi energy $\epsilon_F = -2t$, as seen in Fig. 8 but with artificially suppressed bulk → bulk scattering processes. The first peak belongs to edge-to-edge scattering processes and is sensitive to the momentum transfer q with approximate frequency $\omega_q = v_{F,\text{edge}}q$. The broadened peaks around $\omega = 1.5t$ belong to edge → bulk scattering to the third and fourth bulk bands. It is clearly visible that there is no scattering from the edge states to the second bulk band, which is located at $\omega = 0.5t$.

i.e., have a vanishing matrix element of the Bragg operator. It is possible to predict this behavior from the dispersion of the edge states (see Fig. 3), as one can see that the lowest edge mode, colored in red (a), passes unimpeded through the second bulk band, and never displays an avoided crossing with the blue (b) edge mode of the second band or the second band itself, while it always merges with the third or fourth band (with which we find nonvanishing matrix elements of the Bragg operator). For higher energies and strong confinements, we see the opposite behavior of avoided crossings between red (a) edge modes and yellow (c) edge modes, indicating that one can expect a finite Bragg response from transitions between these states.

Note that the lack of edge → bulk scattering is not a result of the soft-boundaries inhibiting real-space overlap. We have performed equivalent hard-wall boundary calculations where real-space overlap is guaranteed but we again observe an absence of signal for disconnected edge → bulk transitions. Note also, that we do not expect to observe a clear signal for large frequency edge → edge transitions regardless of the type of trap, as there is larger range of states beneath the Fermi-edge that can be accessed with the Bragg laser. Hence, many different values of k_y will contribute, leading to a blurred signal.

V. CONCLUSION

In this article, we analyzed the properties of 2D topological edge states in softly confined systems with a confinement in one direction of the form $V(x) = V_0(x/L)^\delta$. By varying the confining potential from a hard-wall to a quartic or harmonic

potential, we showed that the topological properties of the edge states in specific bulk gaps do not depend on the steepness of the confining potential, while a confinement sharper than harmonic is required to achieve an appreciable bulk region of the lattice. We suggest that quartic confinement is suitable to observe both edge-state and bulk properties, which may be realized by superimposing attractive and repulsive Gaussian beams. Furthermore, we observed the emergence of robust auxiliary edge states, which provide additional structure to edge modes but do not influence the topological quantum numbers. The main feature of these auxiliary states is that they connect edge states which are spatially separated to bulk bands of the system. This provides a mechanism to preserve topological invariance, as soon as the edge states and bulk bands become spatially separated. In these cases the band structure exhibits a series of avoided crossings that act to preserve the topological invariant. An analysis of the spectral density of softly confined systems in real space revealed the splitting and merging of edge states from different bulk bands, which is also indicative of their topological nature.

We also determined the wave functions of eigenstates in a completely trapped system and showed how these depend on the confining potential. With these, we calculated the dynamical structure factor which can, for instance, be measured by Bragg spectroscopy. We found that the dynamical structure factor can reveal the edge and bulk states of the system and their overlap.

In summary, we demonstrated that topological properties in ultracold-atomic systems with artificial gauge fields are not sensitive to the trapping potentials available in optical-lattice experiments and that the edge states of these systems can be clearly detected via Bragg spectroscopy. We believe that soft boundaries provide more detailed insight into details of the behavior of edge states that cannot be observed in hard-wall systems, and are therefore worth investigation in their own right.

ACKNOWLEDGMENTS

We thank Ulf Bissbort, Peter Orth, and Christiane de Morais-Smith for fruitful discussions. M.B. acknowledges support by the German National Academic Foundation and the Stiftung Polytechnische Gesellschaft Frankfurt am Main. This work was supported by the DFG via Sonderforschungsbereich SFB-TR/49 and Forschergruppe FOR 801.

[1] I. Bloch, J. Dalibard, and W. Zwerger, Rev. Mod. Phys. **80**, 885 (2008).
[2] N. R. Cooper, Adv. Phys. **57**, 539 (2008).
[3] Y.-J. Lin, R. L. Compton, A. R. Perry, W. D. Phillips, J. V. Porto, and I. B. Spielman, Phys. Rev. Lett. **102**, 130401 (2009).
[4] Y.-J. Lin, R. L. Compton, K. Jiménez-García, J. V. Porto, and I. B. Spielman, Nature (London) **462**, 628 (2009).
[5] M. Lewenstein, A. Sanpera, V. Ahufinger, B. Damski, A. Sen(de), and U. Sen, Adv. Phys. **56**, 243 (2007).
[6] N. R. Cooper, Phys. Rev. Lett. **106**, 175301 (2011).
[7] D. Jaksch and P. Zoller, New J. Phys. **5**, 56 (2003).
[8] E. J. Mueller, Phys. Rev. A **70**, 041603(R) (2004).
[9] A. S. Sorensen, E. Demler, and M. D. Lukin, Phys. Rev. Lett. **94**, 086803 (2005).
[10] I. B. Spielman, Phys. Rev. A **79**, 063613 (2009).
[11] F. Gerbier and J. Dalibard, New J. Phys. **12**, 033007 (2010).
[12] K. Jiménez-García, L. J. LeBlanc, R. A. Williams, M. C. Beeler, A. R. Perry, and I. B. Spielman, arXiv:1201.6630.
[13] J. Dalibard, F. Gerbier, G. Juzeliūnas, and P. Öhberg, Rev. Mod. Phys. **83**, 1523 (2011).
[14] L.-K. Lim, A. Hemmerich, and C. M. Smith, Phys. Rev. A **81**, 023404 (2010).
[15] Y.-J. Lin, K. Jiménez-García, and I. B. Spielman, Nature **471**, 83 (2011).
[16] N. Goldman, W. Beugeling, and C. M. Smith, Europhys. Lett. **97**, 23003 (2012).
[17] K. Osterloh, M. Baig, L. Santos, P. Zoller, and M. Lewenstein, Phys. Rev. Lett. **95**, 010403 (2005).
[18] J. Ruseckas, G. Juzeliūnas, P. Öhberg, and M. Fleischhauer, Phys. Rev. Lett. **95**, 010404 (2005).
[19] M. Aidelsburger, M. Atala, S. Nascimbène, S. Trotzky, Y. A. Chen, and I. Bloch, Phys. Rev. Lett. **107**, 255301 (2011).
[20] J. Struck, C. Ölschläger, M. Weinberg, P. Hauke, J. Simonet, A. Eckardt, M. Lewenstein, K. Sengstock, and P. Windpassinger, Phys. Rev. Lett. **108**, 225304 (2012).
[21] T. D. Stanescu, V. Galitski, J. Y. Vaishnav, C. W. Clark, and S. Das Sarma, Phys. Rev. A **79**, 053639 (2009).
[22] T. D. Stanescu, V. Galitski, and S. Das Sarma, Phys. Rev. A **82**, 013608 (2010).
[23] N. Goldman, I. Satija, P. Nikolic, A. Bermudez, M. A. Martin-Delgado, M. Lewenstein, and I. B. Spielman, Phys. Rev. Lett. **105**, 255302 (2010).
[24] D. R. Hofstadter, Phys. Rev. B **14**, 2239 (1976).
[25] Y. Hatsugai, Phys. Rev. B **48**, 11851 (1993).
[26] K. v. Klitzing, G. Dorda, and M. Pepper, Phys. Rev. Lett. **45**, 494 (1980).
[27] F. Delahaye, D. Dominguez, Y. Guldner, J. P. Hirtz, M. Razeghi, J. P. Vieren, and J. P. Voos, Phys. Rev. B **33**, 3990 (1986).
[28] M. König, S. Wiedmann, C. Brüne, A. Roth, H. Buhmann, L. W. Molenkamp, X.-L. Qi, and S.-c. Zhang, Science **318**, 766 (2007).
[29] C. L. Kane and E. J. Mele, Phys. Rev. Lett. **95**, 146802 (2005).
[30] B. A. Bernevig and S.-C. Zhang, Phys. Rev. Lett. **96**, 106802 (2006).
[31] M. Kohmoto, Phys. Rev. B **39**, 11943 (1989).
[32] M. Z. Hasan and C. L. Kane, Rev. Mod. Phys. **82**, 3045 (2010).
[33] D. J. Thouless, M. Kohmoto, M. P. Nightingale, and M. den Nijs, Phys. Rev. Lett. **49**, 405 (1982).
[34] Y. Hatsugai, J. Phys.: Condens. Matter **9**, 2507 (1997).
[35] A. M. Essin and V. Gurarie, Phys. Rev. B **84**, 125132 (2011).

[36] The stripe geometry is infinitely extended in the y-direction and as long as translational invariance is not broken along this direction, the Hamiltonian can be expressed in terms of k_y and x. In this case, a 100×100 lattice corresponds to 100 lattice sites in the x-direction and k_y being chosen on a 100 points grid in the interval $[-\pi/a,\pi/a]$.

[37] Please note that the stripe geometry has the discrete translational invariance of an infinite lattice in y-direction and therefore the quasi-momentum k_y is a well defined quantum number.

[38] C. Wu, B. A. Bernevig, and S.-C. Zhang, Phys. Rev. Lett. **96**, 106401 (2006).

[39] C. Xu and J. E. Moore, Phys. Rev. B **73**, 045322 (2006).

[40] The integrated spectral function for the full system can be obtained from $\rho(k_y,\omega) = \rho_L(k_y,\omega) + \rho_R(k_y,\omega)$, where $\rho_R(k_y,\omega)$ is the integrated spectral function for the right half of the system, which fulfills $\rho_R(k_y,\omega) = \rho_L(-k_y,\omega)$.

[41] O. Gygi, H. G. Katzgraber, M. Troyer, S. Wessel, and G. G. Batrouni, Phys. Rev. A **73**, 063606 (2006).

[42] S. Will, T. Best, U. Schneider, L. Hackermüller, D.-S. Lühmann, and I. Bloch, Nature (London) **465**, 197 (2010).

[43] S. Will, T. Best, S. Braun, U. Schneider, and I. Bloch, Phys. Rev. Lett. **106**, 115305 (2011).

[44] L. Fallani, J. E. Lye, V. Guarrera, C. Fort, and M. Inguscio, Phys. Rev. Lett. **98**, 130404 (2007).

[45] J. Billy, V. Josse, Z. Zuo, A. Bernard, B. Hambrecht, P. Lugan, D. Clément, L. Sanchez-Palencia, P. Bouyer, and A. Aspect, Nature **453**, 891 (2008).

[46] L. Sanchez-Palencia and M. Lewenstein, Nat. Phys. **6**, 87 (2010).

[47] In the presence of a disordered background potential, translational invariance in the y-direction is broken and therefore, to mimick a semi-infinite system, we diagonalize the Hamiltonian of the system on a $L_x \times L_y$ lattice with periodic boundary conditions in the y-direction (i.e. $\psi(x,y) = \psi(x,y+L_y)$, where $\psi(x,y)$ is the single-particle wave function).

[48] At this point, one has to keep in mind that we are investigating the properties of a finite system, which has per construction only localized eigenstates. Localization or delocalization therefore means confinement to few lattice sites or an extension over various sites and must be understood from the context.

[49] D. Makogon, I. B. Spielman, and C. Morais-Smith, Europhys. Lett. **97**, 33002 (2012).

[50] N. Goldman, I. Satija, P. Nikolic, A. Bermudez, M. A. Martin-Delgado, M. Lewenstein, and I. B. Spielman, Phys. Rev. Lett. **105**, 255302 (2010).

[51] A. Messiah, *Quantum Mechanics*, Vol. I (Wiley, New York, 1961).

[52] C. Cohen-Tannoudji, B. Diu, and F. Laloë, *Quantum Mechanics* (Wiley, New York, 1977).

[53] V. W. Scarola and S. Das Sarma, Phys. Rev. Lett. **98**, 210403 (2007).

[54] X.-J. Liu, X. Liu, C. Wu, and J. Sinova, Phys. Rev. A **81**, 033622 (2010).

[55] N. Goldman, J. Beugnon, and F. Gerbier, arXiv:1203.1246v1.

[56] T.-L. Dao, A. Georges, J. Dalibard, C. Salomon, and I. Carusotto, Phys. Rev. Lett. **98**, 240402 (2007).

[57] R. O. Umucalilar, H. Zhai, and M. O. Oktel, Phys. Rev. Lett. **100**, 070402 (2008).

[58] E. Zhao, N. Bray-Ali, C. J. Williams, I. B. Spielman, and I. I. Satija, Phys. Rev. A **84**, 063629 (2011).

[59] E. Alba, X. Fernandez-Gonzalvo, J. Mur-Petit, J. K. Pachos, and J. J. Garcia-Ripoll, Phys. Rev. Lett. **107**, 235301 (2011).

[60] D. M. Stamper-Kurn, A. P. Chikkatur, A. Gorlitz, S. Inouye, S. Gupta, D. E. Pritchard, and W. Ketterle, Phys. Rev. Lett. **83**, 2876 (1999).

[61] J. Stenger, S. Inouye, A. P. Chikkatur, D. M. Stamper-Kurn, D. E. Pritchard, and W. Ketterle, Phys. Rev. Lett. **82**, 4569 (1999).

[62] J. Steinhauer, R. Ozeri, N. Katz, and N. Davidson, Phys. Rev. Lett. **88**, 120407 (2002).

[63] J. W. Negele and H. Orland, *Quantum Many-Particle Systems* (Addison-Wesley, Redwood City, CA, 1988).

[64] In this case we used the Fermi velocity $v_F \equiv \partial_{k_y}\epsilon_F(k_y)$ of the edge states of the cylindrical geometry, where k_y is a good quantum number, to approximate the frequency ω, which is reasonable when looking at Fig. 6.